Available online at www.sciencedirect.com
ScienceDirect
Journal of Sound and Vibration 300 (2007) 1015–1033
JOURNAL OF SOUND AND VIBRATION
www.elsevier.com/locate/jsvi

Sesquipoles in aeroacoustics

C.J. Chapman*

Department of Mathematics, University of Keele, Keele, Staffordshire ST5 5BG, UK

Received 30 March 2006; received in revised form 2 September 2006; accepted 12 September 2006
Available online 7 November 2006

Abstract

This paper describes a class of sound fields generated at a sharp edge by fluid flow. These fields, half-way between monopoles and dipoles in both amplitude and directivity, are sesquipoles ('sesqui' being a term for 'one and a half'). Such fields are generated with large amplitude when a high-frequency gust strikes the leading edge of an aerofoil or fan blade, and are important in aeroacoustics. Four basic sesquipoles are identified, the two- and three-dimensional single-frequency sesquipoles, and the two- and three-dimensional impulsive sesquipoles; and four related sesquipoles are constructed from sources whose strength has a Gaussian or top-hat profile in time or along the span. Of these eight fields, seven are new, the previously known field being the two-dimensional single-frequency sesquipole, for which R. Martinez and S.E. Widnall gave an explicit formula in 1983. The results are applicable to studies of turbofan noise.

1. Introduction

This paper is concerned with a type of sound field generated by a convected gust which strikes the leading edge of a high-speed aerofoil or fan blade. This sound generation problem, an example of 'blade–vortex interaction', is of fundamental importance in noise research on turbofan aeroengines (e.g. Refs. [1,2]). The author has obtained an analytical solution [3] of an idealised version of the problem, unifying and generalising previous work [4–8]. The solution gives the full three-dimensional sound field, including the near field, when the gust has arbitrary shape in space and time.

A feature of continuum mechanics is the usefulness of 'basic singular solutions' of the governing equations, containing, for example, delta functions or inverse powers of distance. These solutions are invaluable for constructing Green's function representations of a field quantity, and on their own are accurate away from singularities, e.g. in describing a monopole or dipole field. This paper gives a detailed account of basic singular solutions, half-way between monopoles and dipoles in both amplitude and directivity, of the equations of aeroacoustics. These solutions, which may be called sesquipoles, are perfectly adapted to describing the sound generated at a sharp edge. The paper contrasts with Chapman [9], which, by design, excluded delta functions, using, instead, rise-time and width parameters to describe source and field shapes.

*Tel.: +44 1782 583262; fax: +44 1782 584268.
E-mail address: c.j.chapman@maths.keele.ac.uk.

0022-460X/$ - see front matter
doi:10.1016/j.jsv.2006.09.002

A key aim of the paper is to give a complete account of the directivity patterns of the acoustic field produced by gusts localised in space or time. The directivities are complicated, and depend strongly on the type of gust; hence the paper contains a large number of detailed results for eight different types of gust, including both the near field and far field. For seven of these types of gust, the results are new. One reason that these sound fields have not previously been calculated, despite their fundamental nature in aeroacoustics, is that they require evaluation of Fourier inversion integrals in two complex variables. Since practical methods for evaluating these integrals for leading-edge noise are now available [3], the present paper concentrates on giving a large number of useful results.

The results in the paper are intelligible without reference to the way in which they were derived, i.e. the results can all be understood by acousticians who would not themselves wish to evaluate inversion integrals in the complex plane. Nevertheless, the results are complicated, especially the three-dimensional directivity patterns, and one naturally seeks to apply physical insight to understand the results in physical terms. The most important fact is that the problem is doubly anisotropic, in that there are two special directions, namely the direction of the mean flow and the direction of the leading edge. Moreover, around a sharp leading edge there are singularities in the pressure and velocity fields, of inverse square-root type for a two-dimensional field, but of a far more complicated type for the three-dimensional field around a point singularity on the leading edge. Even when the sound generation is localised to a small segment of the leading edge, the field is still singular all the way along the leading edge, arbitrarily far from the sound generation region. Another important physical fact is the profound difference between near and far fields. These physical aspects of the problem are referred to at various places in the paper. However, for even the most basic quantitative information about the sound field, there is no escape from meticulous analysis of the integral for the pressure. The physics of the sound generation process is buried deep within the phase relations represented by this integral, and no method other than careful mathematical analysis has yet been found for calculating the complete details of sound generation by a gust striking a sharp leading edge.

The sound field generated at the leading edge is diffracted by the trailing edge and side edges, to give a total sound field with in general a multi-lobed far-field directivity pattern. This diffraction process involves the conversion of one sound field into another sound field or into vorticity. The present paper is concerned exclusively with a different process, namely the generation of a sound field from a source which is not acoustic at all, namely vorticity in a mean flow. Therefore the paper does not analyse trailing-edge and side-edge diffraction, or the resulting multi-lobed directivity patterns. Instead, the paper provides a basic building block, namely the three-dimensional and temporal structure of the acoustic field propagating away from the leading edge. With the aid of this building block, a complete directivity pattern, possibly containing many lobes, can be constructed from first principles.

Section 2 of this paper gives the analytical solution in its most general form, and describes two-dimensional single-frequency and impulsive sesquipoles. Sections 3 and 4 describe the corresponding three-dimensional sesquipoles, expressing the results in terms of three 'edgelet functions', denoted E_1, E_2, and E_3. Section 5 describes some smoother sesquipole fields, constructed from sources whose strength has a Gaussian or top-hat profile in time or along the span. Section 6 outlines further work.

2. Leading-edge noise

2.1. General results

The system to be investigated is sketched in Fig. 1, which shows a horizontal flat-plate aerofoil at zero angle of incidence in a uniform horizontal free stream of air at speed U. The speed of sound in the air is c_0, and the Mach number of the flow is $M = U/c_0$. The flow is assumed subsonic, i.e. $M<1$. Cartesian coordinates are chosen so that the origin O is on the leading edge of the aerofoil, the free-stream flow is in the x direction, and the leading edge is the z-axis. The plate occupies the half of the Oxz plane specified by $x>0$, and the vertical direction is Oy. Corresponding cylindrical and spherical coordinates are (r, ϕ, z) and (R, θ, ϕ) as indicated. Final results will be expressed in terms of aeroacoustic coordinates $(\bar{x}, \bar{y}, \bar{z})$ defined by $\bar{x} = x/(1-M^2)$, $\bar{y} = y/(1-M^2)^{1/2}$, $\bar{z} = z/(1-M^2)^{1/2}$. Corresponding polar coordinates $(\bar{r}, \bar{\phi}, \bar{z})$ and $(\bar{R}, \bar{\theta}, \bar{\phi})$

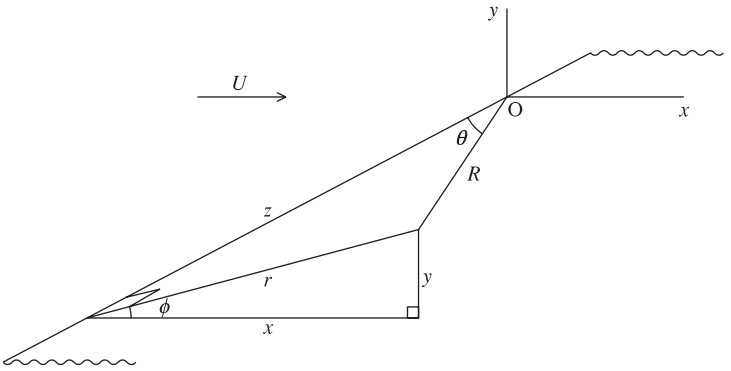

Fig. 1. Flat-plate aerofoil in a uniform flow of speed U; coordinate systems are (x, y, z), (r, ϕ, z), and (R, θ, ϕ). The aerofoil occupies the half-plane $y = 0, x \geqslant 0$ (i.e. $\phi = 0$), and its leading edge is the z-axis (i.e. $\theta = 0, \pi$).

are defined by

$$(\bar{r}, \tan\bar{\phi}) = \left((\bar{x}^2 + \bar{y}^2)^{1/2}, \frac{\bar{y}}{\bar{x}}\right), \quad (\bar{R}, \tan\bar{\theta}) = \left((\bar{r}^2 + \bar{z}^2)^{1/2}, \frac{\bar{r}}{\bar{z}}\right). \tag{1}$$

All formulae for leading-edge noise contain a factor $\cos\frac{1}{2}\bar{\phi}$. This is a distinctive feature of a sesquipole field, because a monopole field would not contain a trigonometric factor, whereas a dipole field would contain a factor such as $\cos\bar{\phi}$.

A small-amplitude convected gust is now superposed on the uniform flow. On inviscid linear theory, the interaction of the gust with the plate occurs only through the vertical component of the gust velocity in the horizontal plane $y = 0$. This component, the upwash, has the functional form $f(t - x/U, z)$. Since the total velocity has zero vertical component on the plate, the boundary-value problem for the acoustic field requires the acoustic velocity on the plate to have vertical component $-f(t - x/U, z)$. Let the undisturbed air have density ρ_0. Then the acoustic velocity $\mathbf{u}$ and the acoustic pressure p may be expressed in terms of a potential $\varphi(t, x, y, z)$ as

$$\mathbf{u} = \boldsymbol{\nabla}\varphi, \quad p = -\rho_0\left(\frac{\partial}{\partial t} + U\frac{\partial}{\partial x}\right)\varphi. \tag{2}$$

The boundary-value problem for φ, obtainable from linearised thin-aerofoil theory, is specified and solved in Chapman [3]. Frequencies are represented by ω, and wavenumbers conjugate to z by m. The convention for Fourier transforms is

$$F(\omega, m) = \int_{-\infty}^{\infty}\int_{-\infty}^{\infty} f(t, z)\mathrm{e}^{\mathrm{i}(\omega t - mz)}\,\mathrm{d}t\,\mathrm{d}z, \tag{3}$$

$$f(t, z) = \frac{1}{4\pi^2}\int_{-\infty}^{\infty}\int_{-\infty}^{\infty} F(\omega, m)\mathrm{e}^{-\mathrm{i}(\omega t - mz)}\,\mathrm{d}\omega\,\mathrm{d}m. \tag{4}$$

The principal result is that the acoustic pressure p is

$$p = \frac{\mathrm{e}^{\pi\mathrm{i}/4}}{4\pi^{5/2}}\frac{\rho_0 c_0 M^{3/2}}{1 - M^2}\frac{\cos\frac{1}{2}\bar{\phi}}{\sin^{1/2}\bar{\theta}}\frac{1}{\bar{R}^{1/2}}\int_{-\infty}^{\infty}\left(\frac{\omega}{c_0}\right)^{1/2}\mathrm{e}^{-\mathrm{i}\omega(t + M\bar{x}/c_0)}$$
$$\times\int_C \frac{\mathrm{e}^{\mathrm{i}(\omega\bar{R}/c_0)\cos(\bar{\theta} - \chi)}\sin\chi}{(1 + M\sin\chi)^{1/2}} F(\omega, (1 - M^2)^{-1/2}(\omega/c_0)\cos\chi)\,\mathrm{d}\chi\,\mathrm{d}\omega. \tag{5}$$

Full details of contours of integration, together with numerous diagrams, are given in Chapman [3]. The contour C is in the χ plane, and the allowed contours C depend on ω. The real part of a complex variable is indicated by a subscript r, and the imaginary part by a subscript i, so that $\chi = \chi_\mathrm{r} + \mathrm{i}\chi_\mathrm{i}$ and $\omega = \omega_\mathrm{r} + \mathrm{i}\omega_\mathrm{i}$.

When ω is real and positive, one choice of C is the rectilinear path in the χ plane from $\pi - \mathrm{i}\infty$ to $\mathrm{i}\infty$ via π and 0. When ω is real and negative, the corresponding contour C in the χ plane is from $-\mathrm{i}\infty$ to $\pi + \mathrm{i}\infty$ via 0 and π. The contour C may be deformed onto the steepest-descent path through the saddle point of the integrand at $\chi = \bar{\theta}$. The branch line of $\omega^{1/2}$ is taken to run from 0 to $-\mathrm{i}\infty$. When ω is real and positive, so is $\omega^{1/2}$. For causality, the ω contour from $-\infty$ to ∞ in Eq. (5) lies above $\omega = 0$. The branch points of $(1 + M\sin\chi)^{1/2}$ are at $\chi = (2n - \frac{1}{2})\pi \pm \mathrm{i}\cosh^{-1}(1/M)$, $n = 0, \pm 1, \pm 2, \ldots$; branch lines point away from the real χ axis.

2.2. Analytic integrations

The upwash is taken to be the product of a longitudinal shape function f_0 and a transverse shape function g, so that $f(t - x/U, z) = f_0(t - x/U)g(z)$. The Fourier transform of f when $x = 0$ is $F(\omega, m) = F_0(\omega)G(m)$ where

$$F_0(\omega) = \int_{-\infty}^{\infty} f_0(t)\mathrm{e}^{\mathrm{i}\omega t}\,\mathrm{d}t, \quad G(m) = \int_{-\infty}^{\infty} g(z)\mathrm{e}^{-\mathrm{i}mz}\,\mathrm{d}z. \tag{6}$$

For example, let $g(z) = 1$, so that there is no dependence, in the gust or field, on the span coordinate z, i.e. the field is two-dimensional. Then $G(m) = 2\pi\delta(m)$ and $F(\omega, m) = 2\pi F_0(\omega)\delta(m)$. In Eq. (5) the χ integration may be performed analytically to give

$$p = -\frac{\mathrm{e}^{\pi\mathrm{i}/4}}{2\pi^{3/2}} \frac{\rho_0 c_0^{3/2} M^{3/2}}{(1-M^2)^{1/2}(1+M)^{1/2}} \frac{\cos\frac{1}{2}\bar{\phi}}{\bar{r}^{1/2}} \int_{-\infty}^{\infty} \omega^{-1/2}\mathrm{e}^{-\mathrm{i}\omega(t + M\bar{x}/c_0 - \bar{r}/c_0)} F_0(\omega)\,\mathrm{d}\omega. \tag{7}$$

The amplitude factor $\bar{r}^{-1/2}$ in Eq. (7) is characteristic of cylindrical spreading in a two-dimensional sound field. Contour plots of pressure often contain alternating ridges of high pressure and valleys of low pressure, forming wavefronts. To describe these, it is convenient to introduce a wavefront coordinate $\bar{r}'$ defined so that the phase in Eq. (7) contains the factor $t - \bar{r}'/c_0$. Thus $\bar{r}' = \bar{r} - M\bar{x} = (1 - M\cos\bar{\phi})\bar{r}$, and Eq. (7) contains

$$t + \frac{M\bar{x}}{c_0} - \frac{\bar{r}}{c_0} = t - \frac{\bar{r}'}{c_0}, \quad \frac{\cos\frac{1}{2}\bar{\phi}}{\bar{r}^{1/2}} = \frac{(1 - M\cos\bar{\phi})^{1/2}\cos\frac{1}{2}\bar{\phi}}{\bar{r}'^{1/2}}. \tag{8}$$

The directivity factor, i.e. the factor containing $\bar{\phi}$, naturally depends on which radial variable is held constant. On a wavefront, specified at a given time by constant $\bar{r}'$, the relevant directivity factor is that on the right-hand side of Eq. $(8)_2$, i.e. is $(1 - M\cos\bar{\phi})^{1/2}\cos\frac{1}{2}\bar{\phi}$. On physical grounds, in the two-dimensional field given by Eq. (7) a wavefront must, in the variables (x, y, z), lie on the surface of a cylinder expanding at the speed of sound c_0 and simultaneously be convected with the mean flow at speed U. This is confirmed by the identity $\bar{r}'^2 = (x - M\bar{r}')^2 + y^2$, so that surfaces of constant $\bar{r}'$ are cylinders, and the value $\bar{r}' = c_0 t$ gives $(c_0 t)^2 = (x - Ut)^2 + y^2$. Equivalently, $\bar{r}'/c_0$ is the acoustic propagation time, in the mean flow, from the point $(0, 0, z)$ on the leading edge to the point (x, y, z).

As a second example involving Eq. (6), let $f_0(t - x/U) = v_0\mathrm{e}^{-\mathrm{i}\omega_0(t - x/U)}$, where v_0 is a vertical component of velocity and ω_0 is a frequency, and let $g(z)$ be arbitrary; i.e. the upwash and field contain the single frequency ω_0. Then $F_0(\omega) = 2\pi v_0\delta(\omega - \omega_0)$ and $F(\omega, m) = 2\pi_0\delta(\omega - \omega_0)G(m)$. The ω integration in Eq. (5) may be performed analytically to give

$$\begin{aligned} p = {} & \frac{\mathrm{e}^{\pi\mathrm{i}/4}}{2\pi^{3/2}} \frac{\rho_0 c_0 v_0 M^{3/2}}{1 - M^2} \frac{\cos\frac{1}{2}\bar{\phi}}{\sin^{1/2}\bar{\theta}} \left(\frac{\omega_0}{c_0\bar{R}}\right)^{1/2} \mathrm{e}^{-\mathrm{i}\omega_0(t + M\bar{x}/c_0)} \\ & \times \int_C \frac{\mathrm{e}^{\mathrm{i}(\omega_0\bar{R}/c_0)\cos(\bar{\theta} - \chi)}\sin\chi}{(1 + M\sin\chi)^{1/2}} G((1 - M^2)^{-1/2}(\omega_0/c_0)\cos\chi)\,\mathrm{d}\chi. \end{aligned} \tag{9}$$

If ω_0 is real and positive, one choice of C is from $\pi - \mathrm{i}\infty$ to $\mathrm{i}\infty$.

2.3. The far field

When $|\omega\bar{R}/c_0| \gg 1$, the dominant contribution to the χ integral in expression (5) for the acoustic pressure p comes from the neighbourhood of the saddle point $\chi = \bar{\theta}$. Standard theory then shows that a simple far-field

approximation to the acoustic pressure, uniform in the polar angle $\bar{\theta}$ from the leading edge, is

$$p \simeq -\frac{1}{2^{3/2}\pi^2}\frac{\rho_0 c_0 M^{3/2}}{1-M^2}\frac{\sin^{1/2}\bar{\theta}\cos\frac{1}{2}\bar{\phi}}{(1+M\sin\bar{\theta})^{1/2}}\frac{1}{\bar{R}}\int_{-\infty}^{\infty} e^{-i\omega(t+M\bar{x}/c_0-\bar{R}/c_0)} \times\left\{1+\frac{iM}{2\sin\bar{\theta}}\frac{c_0}{\omega\bar{R}}\right\}F(\omega,(1-M^2)^{-1/2}(\omega/c_0)\cos\bar{\theta})\,d\omega. \tag{10}$$

The second term in braces is needed when $\bar{\theta}$ is close to 0 or π, i.e. when the observation point is close to the leading edge. The amplitude factor $\bar{R}^{-1}$ in Eq. (10) is characteristic of spherical spreading in a three-dimensional sound field. The corresponding wavefront coordinate $\bar{R}'$, for which the phase term contains the factor $t-\bar{R}'/c_0$, is $\bar{R}'=\bar{R}-M\bar{x}=(1-M\sin\bar{\theta}\cos\bar{\phi})\bar{R}$. Then Eq. (10) contains the directivity and amplitude factor

$$\frac{(1-M\sin\bar{\theta}\cos\bar{\phi})\sin^{1/2}\bar{\theta}\cos\frac{1}{2}\bar{\phi}}{(1+M\sin\bar{\theta})^{1/2}}\frac{1}{\bar{R}'}. \tag{11}$$

The directivity contains also a factor dependent on $\cos\bar{\theta}$, arising from the term in $\cos\bar{\theta}$ in the integrand of Eq. (10). Thus the directivity is rather complex. This is to be expected, because the two special directions in the problem, namely that of the mean flow and that of the leading edge, inevitably make the sound field highly anisotropic. In the variables (x,y,z), a wavefront lies on the surface of a sphere expanding at the speed of sound c_0 and simultaneously convected with the mean flow at speed U. The wavefront coordinate $\bar{R}'$ satisfies the identity $\bar{R}'^2=(x-M\bar{R}')^2+y^2+z^2$, so that surfaces of constant $\bar{R}'$ are spheres, and the value $\bar{R}'=c_0t$ gives $(c_0t)^2=(x-Ut)^2+y^2+z^2$. That is, $\bar{R}'/c_0$ is the acoustic propagation time, in the mean flow, from $(0,0,0)$ to (x,y,z). For brevity, most fields will be written in terms of $\bar{R}$ or $\bar{r}$, but converted to $\bar{R}'$ or $\bar{r}'$ in the discussion of directivity patterns.

2.4. Explicit far fields

Eq. (10) shows that the far acoustic field is always given by a single integral. The second term in braces in Eq. (10) will now be ignored, i.e. it will be assumed that the observation point is not too close to the leading edge. For three types of gust, each involving an arbitrary function, the resulting integral may be evaluated explicitly. The first type is the single-frequency gust, referred to above, for which the upwash is $v_0e^{-i\omega_0(t-x/U)}g(z)$. Then $F(\omega,m)=2\pi v_0\delta(\omega-\omega_0)G(m)$, and Eq. (10) gives

$$p\simeq\frac{-1}{2^{1/2}\pi}\frac{\rho_0c_0v_0M^{3/2}}{1-M^2}\frac{\sin^{1/2}\bar{\theta}\cos\frac{1}{2}\bar{\phi}}{(1+M\sin\bar{\theta})^{1/2}}\frac{1}{\bar{R}}e^{-i\omega_0(t+M\bar{x}/c_0-\bar{R}/c_0)}G((1-M^2)^{-1/2}(\omega_0/c_0)\cos\bar{\theta}). \tag{12}$$

The second type is an impulsive gust for which the upwash is $v_0\delta((t-x/U)/\tau)g(z)$, whence $F(\omega,m)=v_0\tau G(m)$. Then

$$p\simeq\frac{-1}{2^{1/2}\pi}\rho_0c_0\bar{v}_0M^{3/2}\frac{\sin^{1/2}\bar{\theta}\cos\frac{1}{2}\bar{\phi}}{(1+M\sin\bar{\theta})^{1/2}}\frac{c_0\tau}{\bar{R}|\cos\bar{\theta}|}g\left(\frac{-(1-M^2)^{1/2}c_0(t+M\bar{x}/c_0-\bar{R}/c_0)}{\cos\bar{\theta}}\right). \tag{13}$$

Here $\bar{v}_0=v_0/(1-M^2)^{1/2}$. The third type is a gust with upwash $f_0(t-x/U)\delta(z/a)$, where f_0 is arbitrary. This gust is localised to a single span position $z=0$. Thus $F(\omega,m)=aF_0(\omega)$, and Eq. (10) gives

$$p\simeq\frac{-1}{2^{1/2}\pi}\frac{\rho_0c_0M^{3/2}}{(1-M^2)^{1/2}}\frac{\sin^{1/2}\bar{\theta}\cos\frac{1}{2}\bar{\phi}}{(1+M\sin\bar{\theta})^{1/2}}\frac{\bar{a}}{\bar{R}}f_0(t+M\bar{x}/c_0-\bar{R}/c_0). \tag{14}$$

Here $\bar{a}=a/(1-M^2)^{1/2}$. Hence for a gust localised to a single span position, the time-history of the sound pressure at a fixed far-field observation point is proportional to the upwash at that span position, after allowing for the acoustic propagation time $\bar{R}/c_0-M\bar{x}/c_0$, i.e. $\bar{R}'/c_0$, in the uniform flow. At fixed wavefront coordinate $\bar{R}'$, the directivities in Eqs. (12)–(14) contain an extra factor $1-M\sin\bar{\theta}\cos\bar{\phi}$, as in Eq. (11). Far-field approximations of the type in Eq. (14) are accurate as close as one or two wavelengths from the source position. Thus Eq. (14) is immediately useful in providing the incident sound field required for calculating the

diffraction of the leading-edge sound field by the trailing edge and side edges, provided that the frequency is not too low.

2.5. Basic sesquipoles

Four basic fields are obtained from gusts in which the transverse shape function $g(z)$ is 1 or $\delta(z/a)$ and the longitudinal shape function $f_0(t-x/U)$ is $v_0 e^{-i\omega_0(t-x/U)}$ or $v_0\delta((t-x/U)/\tau)$. These fields are of type (i) two-dimensional single-frequency, (ii) two-dimensional impulsive, (iii) three-dimensional single-frequency, and (iv) three-dimensional impulsive, and are the four basic sesquipoles.

For the two-dimensional single-frequency sesquipole, the upwash is $v_0 e^{-i\omega_0(t-x/U)}$, and the pressure field p is given by Eq. (7) with $F_0(\omega) = 2\pi v_0\delta(\omega-\omega_0)$, i.e.

$$p = -\frac{e^{\pi i/4}}{\pi^{1/2}}\frac{\rho_0 c_0 \bar{v}_0 M^{3/2}}{(1+M)^{1/2}}\left(\cos\frac{1}{2}\bar{\phi}\right)\left(\frac{c_0}{\omega_0 \bar{r}}\right)^{1/2} e^{-i\omega_0(t+M\bar{x}/c_0-\bar{r}/c_0)} \tag{15}$$

([4], Eq. 14). At fixed wavefront coordinate $\bar{r}'$, the directivity is $(1-M\cos\bar{\phi})^{1/2}\cos\frac{1}{2}\bar{\phi}$.

For the two-dimensional impulsive sesquipole, the upwash is $v_0\delta((t-x/U)/\tau)$, and the pressure field p is given by Eq. (7) with $F_0(\omega) = v_0\tau$. Evaluation of the integral gives

$$p = -\frac{1}{\pi}\frac{\rho_0 c_0 \bar{v}_0 M^{3/2}}{(1+M)^{1/2}}\left(\cos\frac{1}{2}\bar{\phi}\right)\tau\frac{H_0(t+M\bar{x}/c_0-\bar{r}/c_0)}{\{(\bar{r}/c_0)(t+M\bar{x}/c_0-\bar{r}/c_0)\}^{1/2}}, \tag{16}$$

which in the wavefront coordinate $\bar{r}'$ is proportional to $(1-M\cos\bar{\phi})^{1/2}(\cos\frac{1}{2}\bar{\phi})\{\bar{r}'(t-\bar{r}'/c_0)\}^{-1/2}H_0(t-\bar{r}'/c_0)$. Here H_0 is the Heaviside function, 0 for negative argument and 1 for positive argument. Thus the sound field given by Eq. (16) is confined to the interior of the convected expanding cylinder bounded by the wavefront surface $\bar{r}' = c_0 t$. Expression (16) evaluated on the aerofoil surface, i.e. for $\bar{\phi} = 0$ and 2π, is given in Amiet [5a,b]; but the full expression (16), containing the factor $\cos\frac{1}{2}\bar{\phi}$, appears to be new. As there is no length scale in the formulation of the problem, Eq. (16) may be written in terms of similarity variables $\bar{x}/(c_0 t)$ and $\bar{r}/(c_0 t)$; in these variables, p contains a factor $\rho_0 c_0 \bar{v}_0\tau/t$. This factor gives the scaling law for the time variation of the acoustic pressure at fixed proportional distance from the leading edge to the wavefront $\bar{r}' = c_0 t$.

3. The three-dimensional single-frequency sesquipole

3.1. The edgelet function E_1

The upwash is now $v_0 e^{-i\omega_0(t-x/U)}\delta(z/a)$, so that $G(m) = a$ and $F(\omega, m) = 2\pi v_0\delta(\omega-\omega_0)$. Then Eq. (5) or Eq. (9) gives

$$p = \frac{e^{-\pi i/4}}{2\pi^{1/2}}\rho_0 c_0 \bar{v}_0 M^{3/2}\frac{\cos\frac{1}{2}\bar{\phi}}{\sin^{1/2}\bar{\theta}}\bar{a}\left(\frac{\omega_0}{c_0\bar{R}}\right)^{1/2} e^{-i\omega_0(t+M\bar{x}/c_0)}E_1, \tag{17}$$

where

$$E_1 = E_1(\omega_0\bar{R}/c_0, \bar{\theta}, M) = \frac{i}{\pi}\int_C \frac{e^{i(\omega_0\bar{R}/c_0)\cos(\bar{\theta}-\chi)}\sin\chi}{(1+M\sin\chi)^{1/2}}\,d\chi. \tag{18}$$

The contour C is specified after Eqs. (5) and (9). The right-hand side of Eq. (18) cannot in general be evaluated in terms of known functions, and defines a new function, here named E_1 to suggest 'edge' or 'edgelet'. When $M = 0$, the integral in Eq. (18) reduces to a multiple of $(\sin\bar{\theta})H_1^{(1)}(\omega_0\bar{R}/c_0)$, where $H_1^{(1)}$ is the Hankel function of the first kind of order 1; the factor i/π in Eq. (18) has been chosen so that in E_1 the multiple is unity, i.e.

$$E_1(\omega_0\bar{R}/c_0, \bar{\theta}, 0) = (\sin\bar{\theta})H_1^{(1)}(\omega_0\bar{R}/c_0). \tag{19}$$

Thus in Eq. (17), when $M \ll 1$ the pressure p becomes proportional to $\sin^{1/2}\bar{\theta}$. In this limit, $(\bar{R}, \bar{\theta}, \bar{\phi})$ tends to (R, θ, ϕ), and Eq. (17) is consistent with the fact that

$$R^{-1/2}H_1^{(1)}(\omega_0 R/c_0)(\sin^{1/2}\theta)(\cos\tfrac{1}{2}\phi)e^{-i\omega_0 t} \tag{20}$$

is a separable solution of the wave equation. All the results below have been checked by comparing their limiting form when $M \ll 1$ with the corresponding results obtained by using Eq. (19) at the outset.

A rapid numerical method of evaluating E_1 is to take the contour C to be the steepest-descent path through the saddle point $\chi = \bar{\theta}$ of $\cos(\bar{\theta} - \chi)$. It will be assumed that ω_0 is real and positive. Then the steepest-descent path extends from $\chi = \bar{\theta} + \frac{1}{2}\pi - \mathrm{i}\infty$ to $\chi = \bar{\theta} - \frac{1}{2}\pi + \mathrm{i}\infty$ and has equation $\cos(\bar{\theta} - \chi_\mathrm{r})\cosh\chi_\mathrm{i} = 1$, i.e.

$$\chi_\mathrm{i} = \mathrm{sgn}(\bar{\theta} - \chi_\mathrm{r})\cosh^{-1}(\sec(\bar{\theta} - \chi_\mathrm{r})) \quad (\bar{\theta} - \tfrac{1}{2}\pi < \chi_\mathrm{r} < \bar{\theta} + \tfrac{1}{2}\pi). \tag{21}$$

In Eq. (18) this gives

$$\chi = \chi_\mathrm{r} + \mathrm{i}\,\mathrm{sgn}(\bar{\theta} - \chi_\mathrm{r})\cosh^{-1}\{\sec(\bar{\theta} - \chi_\mathrm{r})\}, \quad \mathrm{d}\chi = \{1 - \mathrm{i}\,\sec(\bar{\theta} - \chi_\mathrm{r})\}\,\mathrm{d}\chi_\mathrm{r}, \tag{22}$$

so that

$$E_1 = -\frac{\mathrm{i}}{\pi}\int_{\bar{\theta}-(1/2)\pi}^{\bar{\theta}+(1/2)\pi} \frac{\mathrm{e}^{\mathrm{i}(\omega_0\bar{R}/c_0)\cos(\bar{\theta}-\chi)}\sin\chi}{(1 + M\sin\chi)^{1/2}}\{1 - \mathrm{i}\,\sec(\bar{\theta} - \chi_\mathrm{r})\}\,\mathrm{d}\chi_\mathrm{r}. \tag{23}$$

Here χ is the function of χ_r specified by Eq. $(22)_1$; the sign change between Eqs. (18) and (23) occurs because the direction of C is from $\bar{\theta} + \frac{1}{2}\pi$ to $\bar{\theta} - \frac{1}{2}\pi$. Numerical evaluation of E_1 using the steepest-descent integral Eq. (23) is almost instantaneous, because of the decay of the integrand away from $\chi = \bar{\theta}$. In this way E_1 was evaluated numerically for many values of $\omega_0\bar{R}/c_0$, $\bar{\theta}$, and M, and the results were examined as contour plots of the real and imaginary parts $E_{1\mathrm{r}}$ and $E_{1\mathrm{i}}$ in a dimensionless meridional plane $(\bar{Z}, \bar{X})$ through the leading edge, where $\bar{Z} = (\omega_0\bar{R}/c_0)\cos\bar{\theta}$, $\bar{X} = (\omega_0\bar{R}/c_0)\sin\bar{\theta}$. Two advantages of such plots over simple directivity plots are first that they show the phase structure of the field, and second that they emphasise the difference in form between the near and far field, and the sharp transition between them. A typical result is shown in Fig. 2, which gives contour plots of $E_{1\mathrm{r}}$ and $E_{1\mathrm{i}}$ for $M = 0.8$. The figure shows clearly the transition from the near field to the far field at values of $\omega_0\bar{R}/c_0$ of about 1 or 2. In this figure, $\bar{\theta}$ is the polar angle from the $\bar{Z}$ axis, i.e. from the leading edge. Thus the figure shows the directivity of E_1, revealing the maximum in the positive $\bar{X}$ direction.

The far-field approximation to E_1, uniform in the polar angle $\bar{\theta}$, is

$$E_1 \simeq \left(\frac{2}{\pi}\right)^{1/2}\frac{\sin\bar{\theta}}{(1 + M\sin\bar{\theta})^{1/2}}\left\{1 + \frac{\mathrm{i}M}{2\sin\bar{\theta}}\frac{c_0}{\omega_0\bar{R}}\right\}\left(\frac{c_0}{\omega_0\bar{R}}\right)^{1/2}\mathrm{e}^{\mathrm{i}(\omega_0\bar{R}/c_0 - 3\pi/4)}. \tag{24}$$

Thus the dominant term is of order $\bar{R}^{-1/2}$, except along the leading edge, $\bar{\theta} = 0$ or π, where the dominant term is of order $\bar{R}^{-3/2}$. An alternative to Eq. (24), equivalent to it in the displayed powers of $\bar{R}$, is obtained from the standard large-argument approximation to the Hankel function $H_1^{(1)}(\omega_0\bar{R}/c_0)$ by eliminating the common term $\mathrm{e}^{\mathrm{i}\omega_0\bar{R}/c_0}$ from this Hankel-function approximation and Eq. (24). The result is

$$E_1 \simeq \frac{\sin\bar{\theta}}{(1 + M\sin\bar{\theta})^{1/2}}\left\{1 + \frac{\mathrm{i}M}{2\sin\bar{\theta}}\frac{c_0}{\omega_0\bar{R}}\right\}H_1^{(1)}(\omega_0\bar{R}/c_0). \tag{25}$$

An advantage of Eq. (25) over Eq. (24) is that Eq. (25) is exact when $M = 0$, i.e. is then no longer simply a far-field approximation. Fig. 3 compares the exact values of $E_{1\mathrm{r}}$ and $E_{1\mathrm{i}}$, given by Eq. (23), with the far-field approximations Eqs. (24) and (25), for $M = 0.8$. In the free-stream direction, $\bar{\theta} = \frac{1}{2}\pi$, the approximations are good when $\omega_0\bar{R}/c_0 \geqslant 2$; along the leading edge, $\bar{\theta} = 0$ or π, they are good when $\omega_0\bar{R}/c_0 \geqslant 3$.

3.2. The acoustic field

Because the function E_1 is so easy to compute from Eq. (23), contour plots of the acoustic pressure p are readily obtained from Eq. (17). It is convenient to work with the scaled acoustic pressure P_1, defined by $p = \rho_0 c_0 \bar{v}_0 M^{3/2}(\omega_0\bar{a}/c_0)P_1$, so that

$$P_1 = \frac{\mathrm{e}^{-\pi\mathrm{i}/4}}{2\pi^{1/2}}\frac{\cos\frac{1}{2}\bar{\phi}}{\sin^{1/2}\bar{\theta}}\left(\frac{c_0}{\omega_0\bar{R}}\right)^{1/2}\mathrm{e}^{-\mathrm{i}\omega_0(t + M\bar{x}/c_0)}E_1. \tag{26}$$

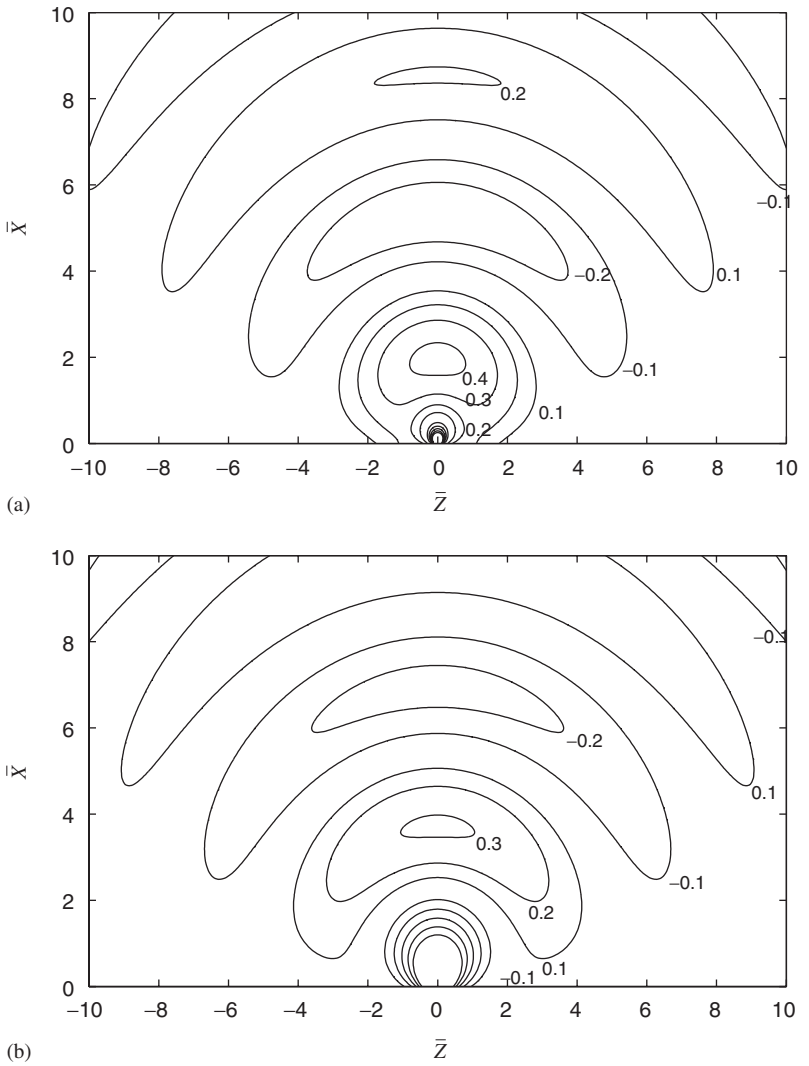

Fig. 2. Contour plots of (a) the real part E_{1r} and (b) the imaginary part E_{1i} of the edgelet function E_1 for $M = 0.8$. The axes are $\bar{Z} = (\omega_0 \bar{R}/c_0)\cos\bar{\theta}$ along the leading edge and $\bar{X} = (\omega_0 \bar{R}/c_0)\sin\bar{\theta}$ in the direction of the free stream. As the origin is approached, $E_{1r} \to -\infty$ and $E_{1i} \to -\infty$; displayed contours near the origin are at values $-0.1(-0.1) - 0.5$ (cf. the leftmost parts of the solid lines in Fig. 3).

Contour plots of P_{1r} and P_{1i} in the half-plane $\bar{\phi} = 0$ at time $t = 0$ for $M = 0.8$ are shown in Fig. 4, and may be contrasted with the contour plots of E_{1r} and E_{1i} in Fig. 2. The free-stream direction $\bar{\theta} = \pi/2$ is a local minimum of the amplitude of P_{1r} and P_{2i}, but a local maximum of the amplitude of E_{1r} and E_{1i}. The explanation lies not only in the term $\sin^{1/2}\bar{\theta}$ in the denominator in Eq. (26), which produces a singularity in P_{1r} and P_{1i} on the leading edge $\bar{\theta} = 0, \pi$, but also in the phase term $\exp(-i\omega_0(t + M\bar{x}/c_0))$. To see this, note that, from Eqs. (24) and (26), the far-field approximation to the scaled acoustic pressure is

$$P_1 \simeq -\frac{1}{2^{1/2}\pi}\frac{\sin^{1/2}\bar{\theta}\cos\frac{1}{2}\bar{\phi}}{(1 + M\sin\bar{\theta})^{1/2}}\left\{1 + \frac{iM}{2\sin\bar{\theta}}\frac{c_0}{\omega_0\bar{R}}\right\}\frac{c_0}{\omega_0\bar{R}}\,e^{-i\omega_0(t + M\bar{x}/c_0 - \bar{R}/c_0)}. \tag{27}$$

A curved ridge or valley in P_{1r} or P_{1i} corresponds to a fixed value of $\omega_0(\bar{R}/c_0 - M\bar{x}/c_0)$, i.e. $\omega_0\bar{R}'/c_0$, where $\bar{R}'$ is the wavefront coordinate defined before Eq. (11). In terms of $\bar{R}'$, the leading term of the far-field

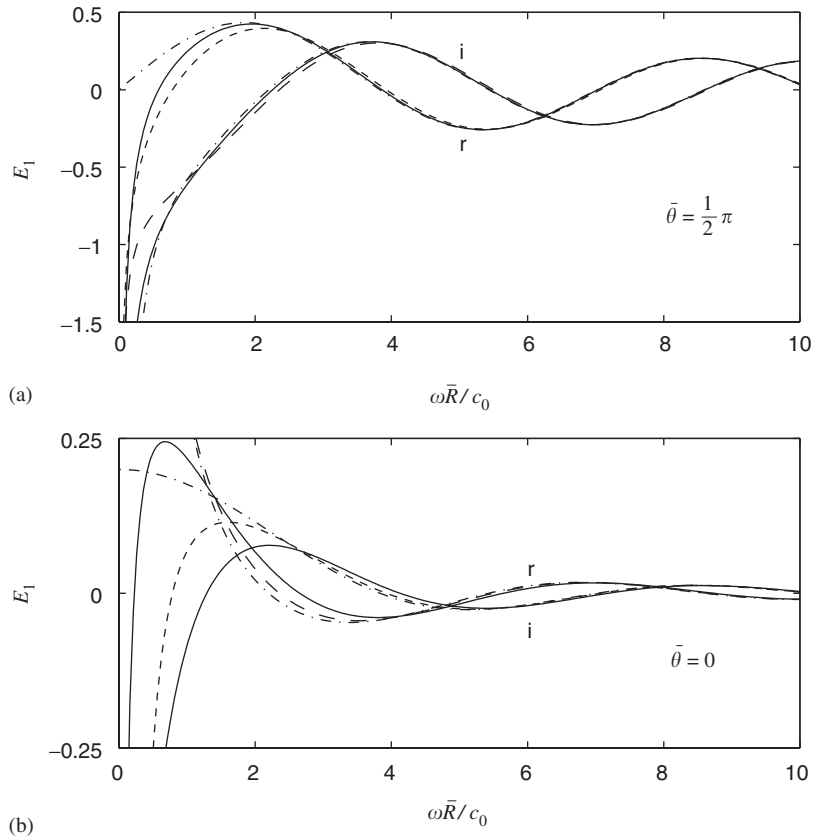

Fig. 3. Exact and approximate values of the edgelet function E_1 for (a) $\bar{\theta} = \frac{1}{2}\pi$, i.e. in the free stream direction, and (b) $\bar{\theta} = 0$, i.e. along the leading edge, for $M = 0.8$. —, exact values given by Eq. (23); – –, standard far-field approximation given by Eq. (24); – ·, Hankel-type far-field approximation given Eq. (25); r, real part E_{1r}; i, imaginary part E_{1i}.

approximation Eq. (27) is

$$P_1 \simeq -\frac{1}{2^{1/2}\pi}\frac{(1 - M\sin\bar{\theta}\cos\bar{\phi})\sin^{1/2}\bar{\theta}\cos\frac{1}{2}\bar{\phi}}{(1 + M\sin\bar{\theta})^{1/2}}\frac{c_0}{\omega_0\bar{R}'}\,\mathrm{e}^{-\mathrm{i}\omega_0(t-\bar{R}'/c_0)}. \tag{28}$$

Therefore the visible pattern of P_{1r} and P_{1i} in Fig. 4 is described by the directivity function

$$D = D(\bar{\theta}) = \frac{(1 - M\sin\bar{\theta}\cos\bar{\phi})\sin^{1/2}\bar{\theta}}{(1 + M\sin\bar{\theta})^{1/2}}, \tag{29}$$

in which $\bar{\phi}$ and M are parameters. The factor $\cos\frac{1}{2}\bar{\phi}$ in Eq. (28) is a constant of proportionality in contour plots at fixed $\bar{\phi}$, and so is not needed in Eq. (29). The derivative $D'(\bar{\theta})$ is zero when $\bar{\theta} = \frac{1}{2}\pi$ and when

$$\cos\bar{\phi} = \frac{1}{M\sin\bar{\theta}\,(3 + 2M\sin\bar{\theta})}. \tag{30}$$

Since $0 \leqslant \bar{\theta} \leqslant \pi$, i.e. $\sin\bar{\theta} \geqslant 0$, it follows that Eq. (30) can be satisfied only for $\cos\bar{\phi} > 0$, and that the relevant solution $\sin\bar{\theta}$ of Eq. (30) is then

$$\sin\bar{\theta} = \frac{(9 + 8\sec\bar{\phi})^{1/2} - 3}{4M}. \tag{31}$$

When $M \leqslant \frac{1}{4}(17^{1/2} - 3) = 0.28078$, the directivity function $D(\bar{\theta})$ has a single maximum, $(1 - M\cos\bar{\phi})/(1 + M)^{1/2}$, attained at $\bar{\theta} = \frac{1}{2}\pi$. When $M > \frac{1}{4}(17^{1/2} - 3)$, the number and location of the maxima depend on $\bar{\phi}$:

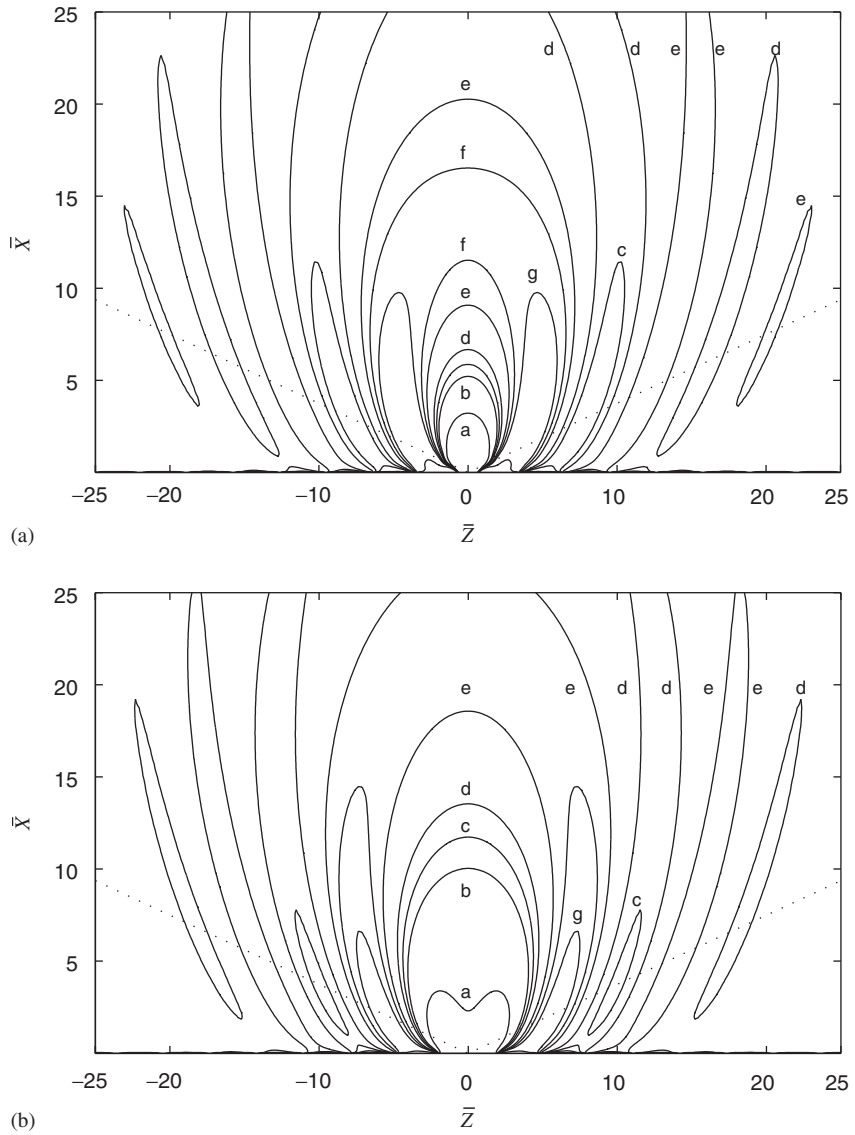

Fig. 4. Contour plots of (a) the real part P_{1r} and (b) the imaginary part P_{1i} of the scaled acoustic pressure P_1 defined by Eq. (26), for $\bar{\phi} = 0$, $t = 0$, $M = 0.8$; cf. E_{1r} and E_{1i} in Fig. 2. The labels (a)–(g) represent contour values -0.040, -0.015, -0.010, -0.005, 0.005, 0.010, 0.015. The dotted lines are in the lobe directions $\bar{\theta} = 20.55^\circ, 159.45^\circ$, as determined by Eq. (31) with $\bar{\phi} = 0$, $M = 0.8$.

for $\cos\bar{\phi} \leqslant 1/\{M(3+2M)\}$ there is a single maximum, still at $\bar{\theta} = \frac{1}{2}\pi$, but for $\cos\bar{\phi} > 1/\{M(3+2M)\}$ there are two maxima, attained at the two values of $\bar{\theta}$ satisfying Eq. (31), and there is now a minimum at $\bar{\theta} = \frac{1}{2}\pi$.

Hence the directivity pattern undergoes a bifurcation from single-lobed to double-lobed as $\cos\bar{\phi}$ increases through $1/\{M(3+2M)\}$, or equivalently as M increases through $\frac{1}{4}\{(9+8\sec\bar{\phi})^{1/2} - 3\}$. The bifurcation is associated with the local maximum in $D(\bar{\theta})$ at $\bar{\theta} = \frac{1}{2}\pi$ undergoing a transition to a local minimum. For the double-lobed pattern, Eq. (31) shows that as $\cos\bar{\phi}$ increases from $1/\{M(3+2M)\}$ to 1, the value of $\sin\bar{\theta}$ at which the maximum is attained decreases from 1 to $\frac{1}{4}(17^{1/2} - 3)/M$; the value of D at each maximum is obtained by substituting Eq. (31) into Eq. (29).

In the special case $\cos\bar{\phi} = 1$, corresponding to observer positions on the blade surface, the directivity pattern is single-lobed for $M \leqslant \frac{1}{4}(17^{1/2} - 3) = 0.28078$ and double-lobed for $M > \frac{1}{4}(17^{1/2} - 3)$; in the latter case the lobe directions are given by $\sin\bar{\theta} = \frac{1}{4}(17^{1/2} - 3)/M$. For $\bar{\phi} = 0$ and $M = 0.8$, this gives

$\sin\bar{\theta} = \frac{5}{16}(17^{1/2} - 3) = 0.35097$, i.e. $\bar{\theta} = 20.55^\circ, 159.45^\circ$. Lines at these angles are superposed on the contour plots of P_{1r} and P_{1i} in Fig. 4; they agree perfectly with the positions of the two lobes.

The directivity analysis based on Eqs. (28)–(31) does not apply when $\sin\bar{\theta}$ is smaller than order $(\omega_0\bar{R}/c_0)^{-1}$, or equivalently when $\omega_0\bar{r}/c_0$ is smaller than order one. For observation points as close as this to the leading edge, the second term in braces in Eq. (27) is important, and at fixed $\bar{R}$ the pressure tends to infinity like $\sin^{-1/2}\bar{\theta}$, or equivalently like $\bar{r}^{-1/2}$, as the leading edge is approached. This pressure singularity is associated with effectively incompressible flow around the sharp leading edge, i.e. with a 'leading-edge near field', extending arbitrarily far along the edge from the source of the sound.

4. The three-dimensional impulsive sesquipole

4.1. The edgelet functions E_2 and E_3

The upwash is now taken to be $v_0\delta((t - x/U)/\tau)\delta(z/a)$. The resulting sound field lies within a convected expanding sphere, generated with radius zero at the origin on the leading edge at time $t = 0$, and then expanding at the speed of sound. The surface of the sphere is the wavefront; outside the sphere there is no sound, and inside the sphere, behind the wavefront, there is a tail acoustic field. A normalised time T is defined so that at any point in space the wavefront arrives at time $T = 1$, and similarly a normalised radial coordinate $\bar{R}_n$ is defined so that the wavefront is always at $\bar{R}_n = 1$. Convenient definitions are

$$T = \frac{c_0 t + M\bar{x}}{\bar{R}}, \quad \bar{R}_n = \frac{\bar{R}}{c_0 t + M\bar{x}} = \frac{1}{T}. \tag{32}$$

Thus for all observer positions there is silence for $T<1$, a wavefront arrival at $T = 1$, and a tail for $T>1$; and for all positive times, there is silence for $\bar{R}_n>1$, a wavefront on $\bar{R}_n = 1$, and a tail for $\bar{R}_n<1$. Inversion of Eq. (32) gives

$$\bar{R} = \frac{c_0 t\bar{R}_n}{1 - M\bar{R}_n\sin\bar{\theta}\cos\bar{\phi}}, \tag{33}$$

so that the wavefront surface $\bar{R}_n = 1$ is $\bar{R} = c_0 t/(1 - M\sin\bar{\theta}\cos\bar{\phi})$. The identity $1 - \bar{R}_n = (c_0 t - \bar{R}')/(c_0 t + M\bar{x})$ shows that the wavefront surface $\bar{R}_n = 1$ is the same as the wavefront surface $\bar{R}' = c_0 t$ defined at the end of Section 2.3; but the formulae below are expressed more simply in terms of $\bar{R}_n$ than $\bar{R}'/(c_0 t)$. For the impulsive problem being considered, the concept of a wavefront is well-defined only at the surface of the expanding sphere $\bar{R}_n = 1$, and not, for example, in its interior $\bar{R}_n<1$.

Because there is no length scale in the formulation of the problem (the quantity a is part of a gust-strength factor $v_0 a\tau$), all formulae relating to the three-dimensional impulsive sesquipole may be written in similarity coordinates $\bar{X}_s = \bar{x}/(c_0 t)$, $\bar{Y}_s = \bar{y}/(c_0 t)$, $\bar{Z}_s = \bar{z}/(c_0 t)$, $\bar{R}_s = \bar{R}/(c_0 t)$. Thus

$$\bar{R}_n = \frac{\bar{R}_s}{1 + M\bar{X}_s} = \frac{\bar{R}_s}{1 + M\bar{R}_s\sin\bar{\theta}\cos\bar{\phi}}. \tag{34}$$

Surfaces of fixed $\bar{R}_n$ are the ellipsoids

$$(1 - M^2\bar{R}_n^2)\left(\bar{X}_s - \frac{M\bar{R}_n^2}{1 - M^2\bar{R}_n^2}\right)^2 + \bar{Y}_s^2 + \bar{Z}_s^2 = \frac{\bar{R}_n^2}{1 - M^2\bar{R}_n^2}. \tag{35}$$

In the untransformed variables $(x/(c_0 t), y/(c_0 t), z/(c_0 t))$ or (x, y, z) these ellipsoids become spherical in the limit $\bar{R}_n \to 1$; and when $\bar{R}_n = 1$ they are the spheres $(c_0 t)^2 = (x - Ut)^2 + y^2 + z^2$. In the variables $(\bar{X}_s, \bar{Y}_s, \bar{Z}_s)$ or $(\bar{x}, \bar{y}, \bar{z})$ the ellipsoids become spherical in the opposite limit $\bar{R}_n \to 0$. By contrast, the surfaces of fixed $\bar{R}'$ used in Section 3.2 for the far field of the single-frequency sesquipole are spheres in the untransformed variables for all $\bar{R}'$.

The pressure field is given by Eq. (5) with $F(\omega, m) = v_0 a\tau$. In terms of the dimensionless frequency variable $\Omega = \omega\bar{R}/c_0$, this gives

$$p = \frac{e^{-\pi i/4}}{4\pi^{3/2}}\rho_0 c_0 \bar{v}_0 M^{3/2}\frac{\cos\frac{1}{2}\bar{\phi}}{\sin^{1/2}\bar{\theta}}\frac{c_0\tau\bar{a}}{\bar{R}^2}\int_{-\infty}^{\infty}\Omega^{1/2}e^{-i\Omega T}E_1(\Omega, \bar{\theta}, M)\,d\Omega. \tag{36}$$

Here E_1 is the edgelet function given by Eq. (18). When $T>1$, i.e. $\bar{R}_n<1$, the Ω contour in Eq. (36) may be deformed downwards and wrapped around the negative imaginary Ω axis. The Ω integration may then be performed analytically at fixed χ, and the remaining χ integral converted to a loop integral around two branch points of $(1+M\sin\chi)^{-1/2}$ in the χ plane. Simplifying gives

$$p=-\frac{1}{2\pi^2}\rho_0 c_0\bar{v}_0 M^{3/2}\frac{\cos\frac{1}{2}\bar{\phi}}{\sin^{1/2}\bar{\theta}}\frac{c_0\tau\bar{a}}{\bar{R}^2}\bar{R}_n^{3/2}E_2\quad(\bar{R}_n<1),\tag{37}$$

where

$$E_2=E_2(\bar{R}_n,\bar{\theta},M)=\mathrm{Re}\int_0^{\chi_M}\frac{\cosh\chi_\mathrm{i}}{(1-M\cosh\chi_\mathrm{i})^{1/2}}\frac{\mathrm{d}\chi_\mathrm{i}}{\{1+\bar{R}_n\sin(\bar{\theta}-\mathrm{i}\chi_\mathrm{i})\}^{3/2}}.\tag{38}$$

Here Re denotes the real part, and $\chi_M=\cosh^{-1}(1/M)$. The value of the three-halves fractional power in the denominator is chosen to be real and positive when the argument is real and positive, and elsewhere is determined by analytic continuation. Eq. (37) is suited to describing the pressure distribution in space at a given time. To describe the pressure history at a given point in space, a more convenient expression is

$$p=-\frac{1}{2\pi^2}\rho_0 c_0\bar{v}_0 M^{3/2}\frac{\cos\frac{1}{2}\bar{\phi}}{\sin^{1/2}\bar{\theta}}\frac{c_0\tau\bar{a}}{\bar{R}^2}E_3\quad(T>1),\tag{39}$$

where

$$E_3=E_3(T,\bar{\theta},M)=\mathrm{Re}\int_0^{\chi_M}\frac{\cosh\chi_\mathrm{i}}{(1-M\cosh\chi_\mathrm{i})^{1/2}}\frac{\mathrm{d}\chi_\mathrm{i}}{\{T+\sin(\bar{\theta}-\mathrm{i}\chi_\mathrm{i})\}^{3/2}}.\tag{40}$$

Since $T=\bar{R}_n^{-1}$, the edgelet functions E_2 and E_3 are related by

$$E_3(T,\bar{\theta},M)=\bar{R}_n^{3/2}E_2(\bar{R}_n,\bar{\theta},M),\quad E_2(\bar{R}_n,\bar{\theta},M)=T^{3/2}E_3(T,\bar{\theta},M).\tag{41}$$

Representation (36) is well suited to describing the field near the wavefront for any M, and to describing the whole field in the low Mach-number limit $M\to 0$. Representations (37) and (39) do not capture the delta function in the pressure field at the wavefront, but are well suited to describing all other aspects of the pressure field. Eq. (34) shows that $\bar{R}_n$, and hence T, are functions of the similarity variables $\bar{X}_s,\bar{R}_s$. In these variables, the above formulae for p contain a factor $\rho_0\bar{v}_0\bar{a}\tau/t^2$, in which c_0 has cancelled out. This factor gives the scaling law for the time variation of the pressure at a fixed proportional distance from the source position to the wavefront.

4.2. The wavefront expansion

It will now be shown that Eq. (36) leads to an expansion

$$p=p_0+p_1+p_2+\cdots,\tag{42}$$

in which p_0 gives the delta-function contribution to the pressure at the wavefront, p_1 gives the pressure immediately behind the wavefront, p_2 gives the rate of change of the pressure (in space or time) immediately behind the wavefront, and so on. Thus p with the term p_0 omitted gives the Taylor expansion, about the wavefront, of the field behind it. The terms in Eq. (42) are

$$p_0=-\frac{1}{2^{1/2}\pi}\rho_0 c_0\bar{v}_0 M^{3/2}(\cos\frac{1}{2}\bar{\phi})\frac{\sin^{1/2}\bar{\theta}}{(1+M\sin\bar{\theta})^{1/2}}\frac{\bar{a}}{\bar{R}}\delta((t+M\bar{x}/c_0-\bar{R}/c_0)/\tau),\tag{43}$$

$$p_1=-\frac{1}{2^{7/2}\pi}\rho_0 c_0\bar{v}_0 M^{3/2}(\cos\frac{1}{2}\bar{\phi})\frac{4M+(3+M^2)\sin\bar{\theta}}{(1+M\sin\bar{\theta})^{5/2}\sin^{1/2}\bar{\theta}}\frac{c_0\tau\bar{a}}{\bar{R}^2}H_0(t+M\bar{x}/c_0-\bar{R}/c_0),\tag{44}$$

$$p_2=\frac{1}{2^{1/2}\pi}\rho_0 c_0\bar{v}_0 M^{3/2}(\cos\frac{1}{2}\bar{\phi})\frac{h_2(\bar{\theta},M)}{\sin^{1/2}\bar{\theta}}\frac{c_0\tau\bar{a}}{\bar{R}^2}\left|\frac{c_0t+M\bar{x}}{\bar{R}}-1\right|H_0(t+M\bar{x}/c_0-\bar{R}/c_0).\tag{45}$$

These expressions may be written in terms of the normalised radial coordinate $\bar{R}_n$ by means of Eq. (33), and the directivities at fixed $\bar{R}_n$ readily obtained. On the wavefront itself, i.e. for $\bar{R}_n = 1$, it was seen after Eq. (33) that $\bar{R} = c_0 t/(1 - M\sin\bar{\theta}\cos\bar{\phi})$; thus p_0 contains a factor $1 - M\sin\bar{\theta}\cos\bar{\phi}$ and $p_0, p_1, \ldots$ contain the factor $(1 - M\sin\bar{\theta}\cos\bar{\phi})^2$.

To derive Eqs. (43)–(45) from Eq. (36), and determine $h_2(\theta, M)$, the starting point is the asymptotic expansion, for large $|\Omega|$, of E_1. By an extension of Eq. (24), this is

$$E_1(\Omega, \bar{\theta}, M) \sim \left(\frac{2}{\pi\Omega}\right)^{1/2} \mathrm{e}^{\mathrm{i}(\Omega - 3\pi/4)} \left(h_0 + \frac{\mathrm{i}h_1}{\Omega} + \frac{h_2}{\Omega^2} + \cdots\right), \tag{46}$$

where

$$h_0 = G, \quad h_1 = -(\tfrac{1}{8}G + \tfrac{1}{2}G''), \quad h_2 = -(\tfrac{9}{128}G + \tfrac{5}{16}G'' + \tfrac{1}{8}G^{(\mathrm{iv})}), \tag{47}$$

and

$$G = G(\bar{\theta}, M) = \frac{\sin\bar{\theta}}{(1 + M\sin\bar{\theta})^{1/2}}, \tag{48}$$

in which the dashes on G indicate differentiation with respect to $\bar{\theta}$. Thus h_0, h_1, $h_2, \ldots$ are determined as functions of $\bar{\theta}$ and M. Term-by-term integration of Eq. (36) then gives Eqs. (42)–(45); the factor $\mathrm{e}^{-\mathrm{i}\Omega(T-1)}$ in the integrand shows that $p = 0$ when $T < 1$, as known already. In the derivation of this wavefront expansion, there is nowhere a far-field approximation. Hence no matter how close the observation point is to the origin, the arrival of the acoustic field is marked by the delta-function term p_0 in the pressure, exactly. Similar remarks apply to $p_1, p_2, \ldots$, which give exact values of the pressure field, its slope, etc., immediately after the wavefront has passed an observation point. Somewhat behind the wavefront, $p_1 + p_2$ gives an approximation to the pressure, which can be steadily improved by inclusion of further terms $p_3, p_4, \ldots$.

The terms $p_1, p_2, \ldots$ are proportional to $\bar{R}^{-2}$, not $\bar{R}^{-1}$, i.e. give that part of the field which does not transport acoustic energy to infinity. Thus if the direct far field only is of interest, then $p_1, p_2, \ldots$ may be ignored, and the entire field may be regarded as given by p_0, i.e. by the delta-function contribution with its spreading factor $\bar{R}^{-1}$. Nevertheless, near-field scattering of $p_1, p_2, \ldots$ by, for example, corners and side edges of a fan blade, will lead to $p_1, p_2, \ldots$ providing an indirect contribution to the far field which could be considerable.

An alternative approach to the wavefront expansion is via Eq. (37) or Eq. (39), involving the edgelet functions E_2 or E_3. Thus, $E_2(\bar{R}_n, \bar{\theta}, M)$ and all its derivatives with respect to $\bar{R}_n$ may be evaluated analytically for $\bar{R}_n = 1$; and similarly for $E_3(T, \bar{\theta}, M)$ and its derivatives with respect to T for $T = 1$. For example (cf. Eq. (44))

$$E_2(1, \bar{\theta}, M) = \frac{\pi}{2^{5/2}} \frac{4M + (3 + M^2)\sin\bar{\theta}}{(1 + M\sin\bar{\theta})^{5/2}}. \tag{49}$$

This leads to $p_1, p_2, \ldots$, but not to p_0; i.e. as indicated at the end of Section 4.1, E_2 and E_3 do not capture the delta function in the pressure at the wavefront. The reason is that E_2 and E_3 are well-defined, i.e. convergent, on each side of the wavefront, and give the analytical continuation, to the region ahead of the wavefront, of the field behind the wavefront. This analytical continuation, being non-zero, is of no physical interest, because ahead of the wavefront there is no acoustic field.

4.3. The tail

The edgelet integrals E_2 and E_3 can in principle be evaluated in terms of elliptic functions with complex arguments, but the results are too unwieldy to be of use, at least for arbitrary $\bar{\theta}$ and M. Instead, it is preferable to evaluate the integrals numerically, and this is made especially rapid by a prior change of variable to eliminate the singularity in the integrand. The result is

$$E_2 = \left(\frac{2}{M}\right)^{1/2} \mathrm{Re} \int_0^{\pi/2} \frac{1 + ((1 - M)/M)\sin^2\psi}{\{1 + \frac{1}{2}((1 - M)/M)\sin^2\psi\}^{1/2}} \frac{\mathrm{d}\psi}{\{1 + \bar{R}_n \sin(\bar{\theta} - \mathrm{i}\chi_i)\}^{3/2}} \tag{50}$$

in which $\chi_i = \cosh^{-1}(1 + ((1-M)/M)\sin^2\psi)$; and E_3 can be written similarly. In accordance with the remarks at the end of Section 4.1, the scaled pressure P_2 is defined by $p = (\rho_0 \bar{v}_0 \bar{a}\tau/t^2)M^{3/2}P_2$. In the similarity variable $\bar{R}_s$ defined before Eq. (34), this gives

$$P_2 = \frac{-1}{2\pi^2}\frac{\cos\frac{1}{2}\bar{\phi}}{\sin^{1/2}\bar{\theta}}\frac{1}{(1+M\bar{R}_s\sin\bar{\theta}\cos\bar{\phi})^{3/2}}\frac{1}{\bar{R}_s^{1/2}}E_2\left(\frac{\bar{R}_s}{1+M\bar{R}_s\sin\bar{\theta}\cos\bar{\phi}},\bar{\theta},M\right). \tag{51}$$

For observer positions in the vertical plane through the source point, i.e. for $\bar{\theta} = \frac{1}{2}\pi$, the edgelet integrals E_2 and E_3 can be evaluated analytically for all $\bar{R}_n$ or T. The result is

$$E_2\left(\bar{R}_n,\frac{1}{2}\pi,M\right) = \frac{2}{(1+M)^{1/2}(1+\bar{R}_n)^{3/2}}\left\{\frac{1+\bar{R}_n}{1-\bar{R}_n}\left(\frac{E(k)}{1-k^2}-K(k)\right)+\frac{E(k)}{1-k^2}\right\}, \tag{52}$$

where $k = \{(1-M)(1-\bar{R}_n)/((1+M)(1+\bar{R}_n))\}^{1/2}$ and $K(k)$ and $E(k)$ are complete elliptic integrals of the first and second kinds. These are given by

$$K(k) = \int_0^{\pi/2}(1-k^2\sin^2\psi)^{-1/2}\,\mathrm{d}\psi = \frac{1}{2}\pi F\left(\frac{1}{2},\frac{1}{2},1,k^2\right), \tag{53}$$

$$E(k) = \int_0^{\pi/2}(1-k^2\sin^2\psi)^{1/2}\,\mathrm{d}\psi = \frac{1}{2}\pi F\left(-\frac{1}{2},\frac{1}{2},1,k^2\right), \tag{54}$$

in which F denotes the hypergeometric function. Corresponding expressions for E_3 are obtained from Eq. (41), i.e., $E_3(T,\frac{1}{2}\pi,M) = T^{-3/2}E_2(T^{-1},\frac{1}{2}\pi,M)$. Substitution of these expressions for E_2 and E_3 into Eqs. (37) and (39) gives the acoustic field in the vertical plane $\bar{\theta} = \frac{1}{2}\pi$. Taylor-series expansions of these expressions in powers of $1-\bar{R}_n$ or $T-1$ agree with Eqs. (44)–(45) evaluated at $\bar{\theta} = \frac{1}{2}\pi$. In particular, $E_2(1,\frac{1}{2}\pi,M) = 2^{-5/2}\pi(3+M)/(1+M)^{3/2}$, from Eq. (49) or Eq. (52). The edgelet integrals do not simplify for $\bar{\theta} = 0$.

Contour plots of E_2 and P_2 for $M = 0.8$ in the half-plane $\bar{\phi} = 0$, i.e. on the upper surface of the blade, are shown in Fig. 5(a,b); contours of $\bar{R}_n$ are superposed. The polar angle from the $\bar{Z}$-axis, i.e. from the leading edge, is $\bar{\theta}$. Therefore the figure determines the directivity in $\bar{\theta}$ of E_2 and P_2 for $\bar{\phi} = 0$. Corresponding graphs of E_2 and P_2 as functions of $\bar{R}_n$ at fixed $\bar{\theta}$ and as functions of $\bar{\theta}$ at fixed $\bar{R}_n$ are shown in Fig. 6(a–d). Plots in the vertical plane $\bar{\theta} = \frac{1}{2}\pi$ are shown in Fig. 7(a,b), again with contours of $\bar{R}_n$ superposed. Corresponding graphs of P_2 as a function of $\bar{R}_n$ at fixed $\bar{\phi}$ and as a function of $\bar{\phi}$ at fixed $\bar{R}_n$ are shown in Fig. 8(a,b).

4.4. The very near field

When $\bar{R}_n \ll 1$, the integrand of E_2 may be approximated by the first few terms in its Taylor series in powers of $\bar{R}_n$, and integrated term-by-term. The result is

$$E_2 = \frac{2(1+M)^{1/2}}{M}\left\{E(k)-\frac{M}{1+M}K(k)\right\} - \frac{2(1+M)^{1/2}}{M^2}(\sin\bar{\theta})\bar{R}_n\left\{E(k)-\frac{M(2-M)}{2(1+M)}K(k)\right\}+\cdots, \tag{55}$$

where $k = \{(1-M)/(1+M)\}^{1/2}$. For $\bar{\theta} = \frac{1}{2}\pi$, this agrees with the Taylor-series expansion of Eq. (52). Use of Eq. (55) in Eq. (37) gives a near-field approximation to the acoustic pressure. The approximation is good up to about $\bar{R}_n = 0.2$. Equivalently, the relation $E_3(T,\bar{\theta},M) = T^{-3/2}E_2(T^{-1},\bar{\theta},M)$ determines the large-time behaviour of the pressure at a fixed observation point. The pressure decays in proportion to $T^{-3/2}$.

4.5. The low Mach-number limit

When $M \ll 1$, the above formulae simplify, because Eq. (19) gives $E_1(\Omega,\bar{\theta},0) = (\sin\bar{\theta})H_1^{(1)}(\Omega)$. The large $|\Omega|$ expansion of E_1 is then obtainable from that of $H_1^{(1)}(\Omega)$; this agrees with Eq. (46) for $M = 0$. The value

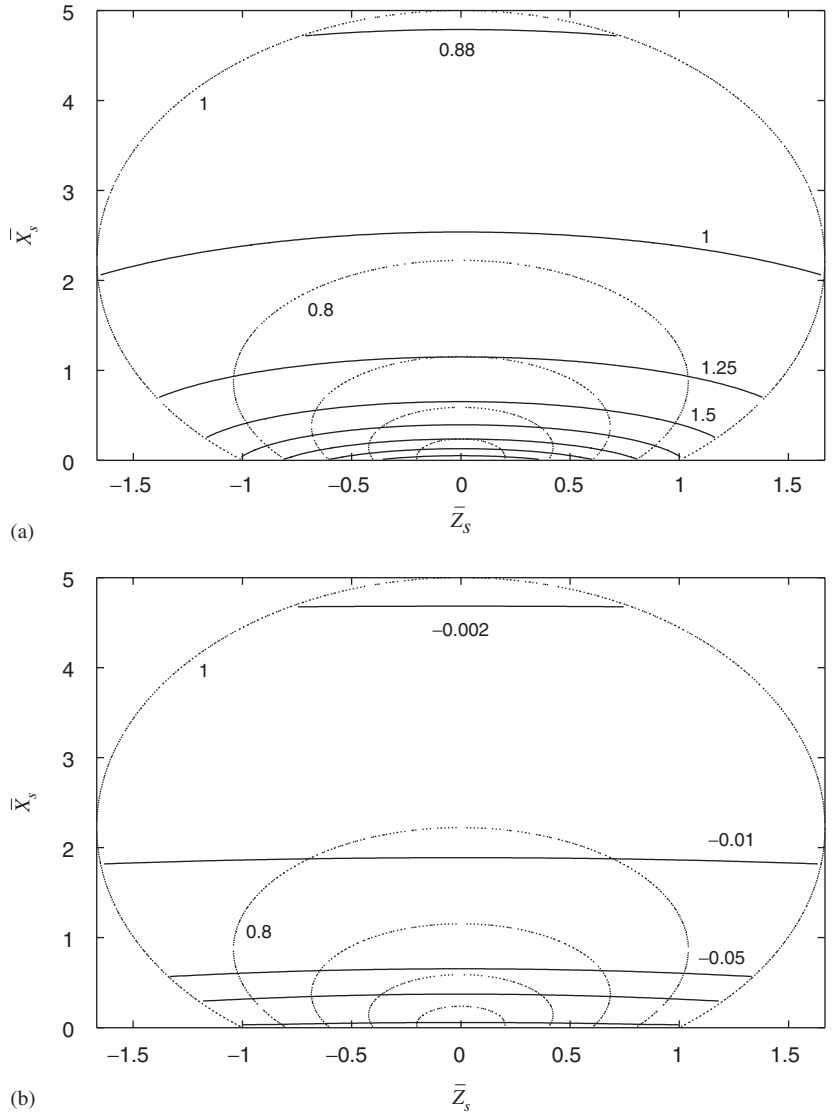

Fig. 5. (a) Contours of E_2 (solid lines) for $M = 0.8$ in the half-plane $\bar{\phi} = 0$, i.e. on the upper surface of the blade; dotted lines are contours of $\bar{R}_n$. Contour values of E_2 are 0.88, 1.00(0.25)2.5, and of $\bar{R}_n$ are 0.2(0.2)1.0. The axes are $\bar{Z}_s = \bar{z}/(c_0 t)$, along the leading edge, and $\bar{X}_s = \bar{x}/(c_0 t)$, in the free stream direction. (b) As (a), but for P_2; contour values are $-0.002, -0.01, -0.05, -0.1, -0.5$.

of $E_2(\bar{R}_n, \theta, 0)$ is given by Eq. (38) with $M = 0$; alternatively, the Ω integration described after Eq. (36) leads to

$$E_2(\bar{R}_n, \bar{\theta}, 0) = \frac{2}{\pi^{1/2}} \frac{\sin\bar{\theta}}{\bar{R}_n^{3/2}} \int_0^\infty s^{1/2} \mathrm{e}^{-s/\bar{R}_n} K_1(s)\,\mathrm{d}s \quad (\bar{R}_n < 1), \tag{56}$$

in which K_1 is the modified Bessel function of order 1. The s integral may be evaluated analytically, and the result expressed in several equivalent ways, involving Legendre functions $P^{\pm 1}_{1/2}(\bar{R}_n^{-1})$ or $Q^{\pm 1}_{1/2}((1-\bar{R}_n^2)^{-1/2})$, or hypergeometric functions with argument $1 - \bar{R}_n^2$ or $(1 - \bar{R}_n)/(1 + \bar{R}_n)$. The latter give

$$\begin{aligned} E_2(\bar{R}_n, \bar{\theta}, 0) &= \frac{3\pi \sin\bar{\theta}}{2^{5/2}\bar{R}_n} F\left(\frac{1}{4}, \frac{3}{4}, 2, 1 - \bar{R}_n^2\right) = \frac{3\pi \bar{R}_n \sin\bar{\theta}}{2^{5/2}} F\left(\frac{5}{4}, \frac{7}{4}, 2, 1 - \bar{R}_n^2\right) \\ &= \frac{3\pi \sin\bar{\theta}}{4\bar{R}_n(1+\bar{R}_n)^{1/2}} F\left(-\frac{1}{2}, \frac{1}{2}, 2, \frac{1-\bar{R}_n}{1+\bar{R}_n}\right) = \frac{3\pi \bar{R}_n \sin\bar{\theta}}{(1+\bar{R}_n)^{5/2}} F\left(\frac{3}{2}, \frac{5}{2}, 2, \frac{1-\bar{R}_n}{1+\bar{R}_n}\right). \end{aligned} \tag{57}$$

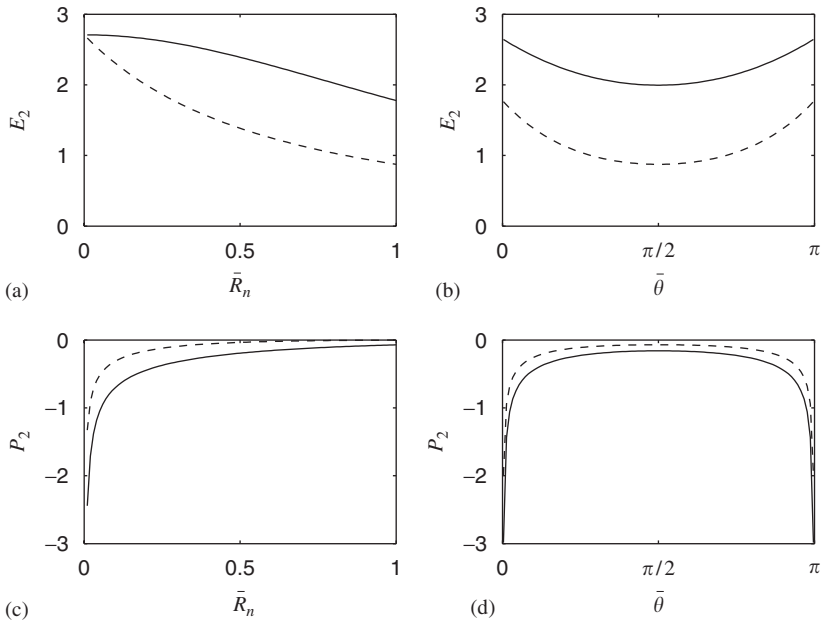

Fig. 6. E_2 and P_2 as functions of $\bar{R}_n$ at fixed $\bar{\theta}$, and as functions of $\bar{\theta}$ at fixed $\bar{R}_n$, obtained from Fig. 5 ($M = 0.8, \bar{\phi} = 0$). (a) —, $\bar{\theta} = 0$; – –, $\bar{\theta} = \frac{1}{2}\pi$; (b),(d) —, $\bar{R}_n = 0.2$; – –, $\bar{R}_n = 1$; (c) —, $\bar{\theta} = \frac{1}{10}\pi$; – –, $\bar{\theta} = \frac{1}{2}\pi$. In relation to Fig. 5, $\bar{\theta} = 0$ is the right half of the $\bar{Z}_s$-axis, on the leading edge, and $\bar{\theta} = \frac{1}{2}\pi$ is $\bar{Z}_s = 0$, in the free stream direction.

Then Eq. (41) gives similar expressions for $E_3(T, \bar{\theta}, 0)$. These expressions evaluated at $\bar{\theta} = \frac{1}{2}\pi$ agree with Eq. (52) evaluated at $M = 0$. Expansion of Eq. (57) in powers of $1 - \bar{R}_n$ leads to the wavefront expansion of Section 4.2, evaluated for $M \to 0$; the leading term is $E_2(1, \bar{\theta}, 0) = (3\pi/2^{5/2}) \sin\bar{\theta}$, and, for example, $h_2(\bar{\theta}, 0) = \frac{15}{128} \sin\bar{\theta}$. Near-field expansions of Eq. (56) or Eq. (57) for $\bar{R}_n \ll 1$ give

$$E_2(\bar{R}_n, \bar{\theta}, 0) = \frac{2\sin\bar{\theta}}{\bar{R}_n}\left\{1 + \left(\frac{3}{8}\ln\left(\frac{1}{8}\bar{R}_n\right) + \frac{13}{16}\right)\bar{R}_n^2 + O(\bar{R}_n^4 \ln \bar{R}_n)\right\}. \tag{58}$$

In formulae for the pressure when $M \ll 1$, the leading-order approximation is obtained by putting $M = 0$ in every term except the leading factor $M^{3/2}$.

5. Smoother fields

The acoustic field analysed in Section 4 is produced by a gust with delta-function profiles both in time and along the span. This section indicates how the field is modified if one of these profiles is smoothed to a Gaussian or top-hat shape; comparison of the results below shows in detail how the shape of the sound field depends on the fine-scale shape of the gust.

For Gaussian time variation, the upwash is $v_0 \mathrm{e}^{-(1/2)\{(t-x/U)/\tau\}^2}\delta(z/a)$, and Eq. (14) gives the far-field approximation

$$p \simeq -\frac{1}{2^{1/2}\pi}\rho_0 c_0 \bar{v}_0 M^{3/2} \frac{\sin^{1/2}\bar{\theta}\cos\frac{1}{2}\bar{\phi}}{(1 + M\sin\bar{\theta})^{1/2}} \frac{\bar{a}}{\bar{R}} \mathrm{e}^{-(1/2)\{(t+M\bar{x}/c_0 - \bar{R}/c_0)/\tau\}^2}. \tag{59}$$

The field at an arbitrary position is given by Eq. (5) with $F(\omega, m) = (2\pi)^{1/2} v_0 \tau \mathrm{e}^{-(1/2)(\omega\tau)^2}$; the ω integration can be performed analytically, to give an expression involving the modified Bessel functions $I_{\pm 1/4}(\frac{1}{4}\{(t + M\bar{x}/c_0 - (\bar{R}/c_0)\cos(\bar{\theta} - \chi))/\tau\}^2)$ and their derivatives. The remaining χ integral may be evaluated numerically.

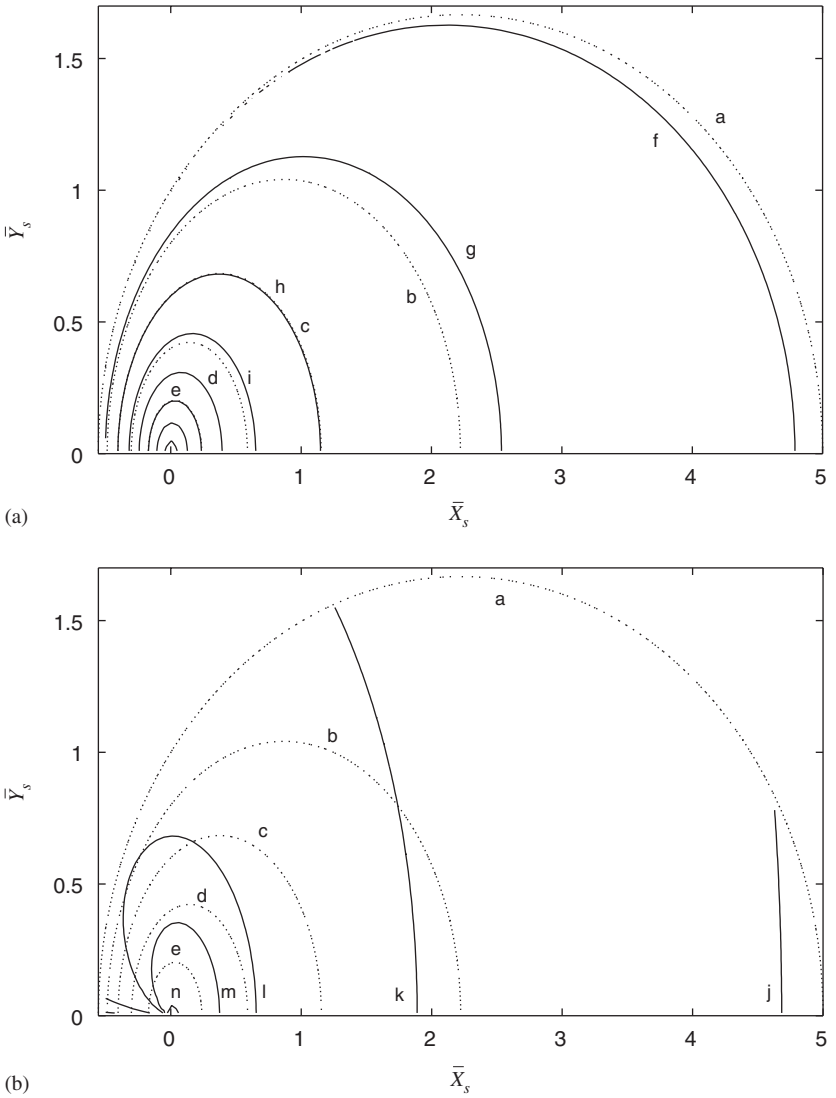

Fig. 7. (a) Contours of E_2 (solid lines) for $M = 0.8$ in the vertical plane $\bar{\theta} = \frac{1}{2}\pi$; dotted lines are contours of $\bar{R}_n$. Contour values of E_2 are (f) 0.88; (g) 1; (h) 1.25; (i) 1.25; and 1.5, 2, 2.25, 2.5 (unmarked); contour values of $\bar{R}_n$ are (a) 1; (b) 0.8; (c) 0.6; (d) 0.4; (e), 0.2. The axes are $\bar{X}_s$ in the free steam direction and $\bar{Y}_s$ vertically upwards. (b) As (a), but for P_2; contour values are (j) -0.002; (k) -0.01; (l) -0.05; (m) -0.1; (n) -0.5. The contour values are the same as in Fig. 5; thus the level surfaces of E_2 and P_2 in space may be visualised.

For top-hat time variation, the upwash is $v_0 H((t - x/U)/\tau, -1, 1)\delta(z/a)$, where the top-hat function H is defined so that $H(\xi, \xi_0, \xi_1)$ takes the value 1 for $\xi_0 < \xi < \xi_1$ and 0 otherwise. Thus at the fixed point $z = 0$ on the leading edge, the gust lasts a time 2τ. The far-field approximation to the pressure is

$$p \simeq -\frac{1}{2^{1/2}\pi}\rho_0 c_0 \bar{v}_0 M^{3/2} \frac{\sin^{1/2}\bar{\theta}\cos\frac{1}{2}\bar{\phi}}{(1 + M\sin\bar{\theta})^{1/2}} \frac{\bar{a}}{\bar{R}} H((t + M\bar{x}/c_0 - \bar{R}/c_0)/\tau, -1, 1). \tag{60}$$

The field at an arbitrary position is given by Eq. (5) with $F(\omega, m) = 2v_0 a\omega^{-1}\sin\omega\tau$. Analytic integration with respect to ω gives terms in $\{t \pm \tau + M\bar{x}/c_0 - (\bar{R}/c_0)\cos(\bar{\theta} - \chi)\}^{-1/2}$, so that results as complete as those of Section 4 are readily obtained. This involves integrals similar to E_2 and E_3 in Eq. (38) and Eq. (40), but with exponent $\frac{1}{2}$ instead of $\frac{3}{2}$ in the denominators of the integrands.

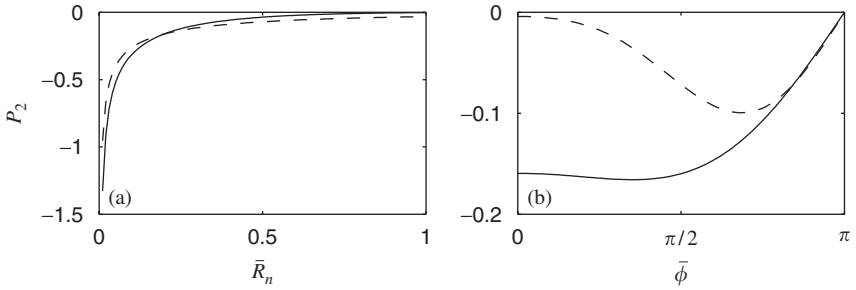

Fig. 8. P_2 as a function of $\bar{R}_n$ at fixed $\bar{\phi}$, and as a function of $\bar{\phi}$ at fixed $\bar{R}_n$, obtained from Fig. 7(b) ($M = 0.8, \bar{\theta} = \frac{1}{2}\pi$). (a) —, $\bar{\phi} = 0$; – –, $\bar{\phi} = \frac{1}{2}\pi$; (b) —, $\bar{R}_n = 0.2$; – –, $\bar{R}_n = 1$. In relation to Fig. 7(b), $\bar{\phi} = 0$ is the right half of the $\bar{X}_s$ axis, in the free stream direction, and $\bar{\phi} = \frac{1}{2}\pi$ is $\bar{X}_s = 0$, vertically upwards.

For Gaussian span variation, the upwash is $v_0\delta((t - x/U)/\tau)g(z)$, where $g(z) = \mathrm{e}^{-(1/2)(z/a)^2}$. Thus Eq. (13) gives the far-field approximation

$$p \simeq -\frac{1}{2^{1/2}\pi}\rho_0 c_0 \bar{v}_0 M^{3/2}\frac{\sin^{1/2}\bar{\theta}\cos\frac{1}{2}\bar{\phi}}{(1+M\sin\bar{\theta})^{1/2}}\frac{c_0\tau}{\bar{R}|\cos\bar{\theta}|}\exp\left\{-\frac{1}{2}\left(\frac{t+M\bar{x}/c_0-\bar{R}/c_0}{(\bar{a}/c_0)\cos\bar{\theta}}\right)^2\right\}. \tag{61}$$

The singularity in this expression when, simultaneously, $\bar{R} - M\bar{x} = c_0 t$, i.e. $\bar{R}' = c_0 t$, and $\bar{\theta} = \frac{1}{2}\pi$, occurs because sound production is confined to the time instant $t = 0$; thus the field has a large in-phase component in the vertical plane through the point of maximum source strength, i.e. through the point $z = 0$ on the leading edge. The field at an arbitrary position is given by Eq. (5) with $F(\omega, m) = (2\pi)^{1/2}v_0 a\tau \mathrm{e}^{-(1/2)(ma)^2}$; the ω integration gives expressions in $I_{\pm 1/4}(\frac{1}{4}\{(t + M\bar{x}/c_0 - (\bar{R}/c_0)\cos(\bar{\theta} - \chi))/((\bar{a}/c_0)\cos\chi)\}^2)$ and their derivatives, which may be integrated numerically with respect to χ.

For top-hat span variation, the upwash is $v_0\delta((t - x/U)/\tau)g(z)$, where $g(z) = H(z/a, -1, 1)$. Thus Eq. (13) gives the far-field approximation

$$p \simeq -\frac{1}{2^{1/2}\pi}\rho_0 c_0 \bar{v}_0 M^{3/2}\frac{\sin^{1/2}\bar{\theta}\cos\frac{1}{2}\bar{\phi}}{(1+M\sin\bar{\theta})^{1/2}}\frac{c_0\tau}{\bar{R}|\cos\bar{\theta}|}H\left(\frac{t+M\bar{x}/c_0-\bar{R}/c_0}{(\bar{a}/c_0)\cos\bar{\theta}}, -1, 1\right), \tag{62}$$

again with singularities in the plane $\bar{\theta} = \frac{1}{2}\pi$. The field at an arbitrary position is given by Eq. (5) with $F(\omega, m) = 2v_0\tau m^{-1}\sin ma$. Integration with respect to ω gives terms in $\{t + M\bar{x}/c_0 - (\bar{R}/c_0\cos(\bar{\theta} - \chi)\pm)(\bar{a}/c_0)\cos\chi\}^{-1/2}$, so that results as complete as those in Section 4 can be obtained. At fixed wavefront coordinate $\bar{R}'$, the directivities in Eqs. (59)–(62) contain an extra factor $1 - M\sin\bar{\theta}\cos\bar{\phi}$, as in Eq. (11).

6. Conclusions and further work

This paper gives detailed information about the most basic sesquipole sound fields which occur in the aeroacoustics of subsonic flow. Corresponding results for supersonic flow have been obtained by Powles [10a–c]; further work would be needed for transonic flow. The results may be extended to account for leading-edge curvature, mean loading, and aerofoil camber by the methods in, for example, Myers and Kerschen [11] and Peake and Kerschen [12]. Further calculations would determine the effect of diffraction of the near field by trailing and side edges, and tips, to give multi-lobed acoustic directivity patterns. The effect of finite span may be modelled approximately by a Kirchhoff-type approximation [13]; an alternative method is to use the loading distribution near the tips [14].

The results may be useful in computational aeroacoustics, because they provide a transfer function between an incoming gust and an acoustic source term. Such a transfer function is needed because for leading-edge noise the acoustic field is not a dipole field generated by the net loading on a blade.

Acknowledgements

The author thanks C.J. Powles for helpful comments.

References

[1] N. Peake, E.J. Kerschen, Influence of mean loading on noise generated by the interaction of gusts with a cascade: downstream radiation, *Journal of Fluid Mechanics* 515 (2004) 99–133.
[2] A.J. Cooper, N. Peake, Upstream-radiated rotor–stator interaction noise in mean swirling flow, *Journal of Fluid Mechanics* 523 (2005) 219–250.
[3] C.J. Chapman, High-speed leading-edge noise, *Proceedings of the Royal Society of London A* 459 (2003) 2131–2151.
[4] R. Martinez, S.E. Widnall, An aeroacoustic model for high-speed unsteady blade–vortex interaction, *AIAA Journal* 21 (1983) 1225–1231.
[5] [a] R.K. Amiet, Airfoil gust response and the sound produced by airfoil–vortex interaction, *Journal of Sound and Vibration* 107 (1986) 487–506;
[b] R.K. Amiet, Gust response of a flat-plate aerofoil in the time domain, *Quarterly Journal of Mechanics and Applied Mathematics* 39 (1986) 485–505.
[6] M.S. Howe, Contributions to the theory of sound production by vortex–airfoil interaction, with application to vortices with finite axial velocity defect, *Proceedings of the Royal Society of London A* 420 (1988) 157–182.
[7] Y.P. Guo, A note on sound from the interruption of a cylindrical flow by a semi-infinite aerofoil of subsonic speed, *Journal of Sound and Vibration* 128 (1989) 275–286.
[8] S.J. Majumdar, N. Peake, Noise generation by the interaction between ingested turbulence and a rotating fan, *Journal of Fluid Mechanics* 359 (1988) 181–216.
[9] C.J. Chapman, Some benchmark problems for computational aeroacoustics, *Journal of Sound and Vibration* 270 (2004) 495–508.
[10] [a] C.J. Powles, Noise generation by a supersonic leading edge, part 1: general theory, *Journal of Sound and Vibration* 276 (2004) 837–852;
[b] C.J. Powles, Noise generation by a supersonic leading edge, part 2: examples of two-dimensional sound fields, *Journal of Sound and Vibration* 276 (2004) 853–868;
[c] C.J. Powles, Supersonic Leading-edge Noise, Ph.D. Thesis, University of Keele, 2004, Staffordshire, UK.
[11] M.R. Myers, E.J. Kerschen, Influence of incidence angle on sound generation by airfoils interacting with high-frequency gusts, *Journal of Fluid Mechanics* 292 (1995) 271–304.
[12] N. Peake, E.J. Kerschen, Influence of mean loading on noise generated by the interaction of gusts with a flat-plate cascade: upstream radiation, *Journal of Fluid Mechanics* 347 (1997) 315–346.
[13] R.K. Amiet, Acoustic radiation from an airfoil in a turbulent stream, *Journal of Sound and Vibration* 41 (1975) 407–420.
[14] N. Peake, The scattering of vorticity waves by a supersonic rectangular wing, *Wave Motion* 25 (1997) 369–383.